During the deposition, the accreting ice layer was irradiated by UV from a microwave-stimulated hydrogen flow discharge lamp (output, $F \approx 1.5 \times 10^{15}$ photons s^{-1} (ref. 31); photon energy, $E_{photon} = 7.3–10.5$ eV, with main emission at Lyman-α (10.2 eV)). The lamp spectrum roughly resembles the UV emission from early-type stars, which dominates the interstellar radiation field between 0.09 and 0.25 μm (ref. 20). The UV-irradiation/deposition typically lasted 24 hours. The total gas flow was $F \approx 1 \times 10^{16}$ molecules s^{-1}, implying an average UV dose of 0.15 photons per molecule. Subsequently, the system was warmed at 1 K min^{-1} to $T = 40$ K using a temperature controller (Scientific Instruments 9600-1), and then at about 4 K min^{-1} up to room temperature. The aluminium block with the residue was removed from the system and stored inside a capsule in a nitrogen atmosphere.

Analytical procedure

A 100-μl water extract of the above produced residue was hydrolysed in 6 M HCl at 110 °C for 24 h under argon atmosphere. This is a standard procedure for hydrolysis of peptides and has been used for the detection of amino acids in meteorites[7]. After evaporation of 6 M HCl, the residues were dissolved in 0.1 M HCl and derivatized using the procedure of ref. 24, leading to amino acid ECEE derivatives. The identities of the amino acid peaks were verified by comparing the retention times and the mass spectra with external standards, purchased from Fluka. By using the single ion monitoring mode, it was possible to select a given ion mass, characteristic of the target amino acid in order to increase both chromatographic resolution and sensitivity. The determination of the signal-to-noise ratio for each amino acid was performed in the extract ion mode.

Received 16 November 2001; accepted 17 January 2002.

1. Bar-Nun, A. & Chang, S. Photochemical reactions of water and carbon monoxide in Earth's primitive atmosphere. *J. Geophys. Res.* **88,** 6662–6672 (1983).
2. Oró, J. Comets and the formation of biochemical compounds on the primitive Earth. *Nature* **190,** 389–390 (1961).
3. Greenberg, J. M. in *The Galaxy and the Solar System* 103–115 (Univ. Arizona Press, Tucson, 1986).
4. Brack, A. Life in the Solar System. *Adv. Space. Res.* **24,** 417–433 (1999).
5. Meierhenrich, U., Thiemann, W.H.-P. & Rosenbauer, H. Molecular parity violation via comets?*Chirality* **11,** 575–582 (1999).
6. Engel, M. H. & Macko, S. A. The stereochemistry of amino acids in the Murchison meteorite. *Precambr. Res.* **106,** 35–45 (2001).
7. Kvenvolden, K. A. *et al.* Evidence for extraterrestrial amino acids and hydrocarbons in the Murchison meteorite. *Nature* **228,** 923–926 (1970).
8. Cronin, J. R. & Pizzarello, S. Enantiomeric excesses in meteoritic amino acids. *Science* **275,** 951–955 (1997).
9. Ehrenfreund, P., Glavin, D. P., Botta, O., Cooper, G. & Bada, J. L. Extraterrestrial amino acids in Orgueil and Ivuna: Tracing the parent body of CI type carbonaceous chondrites. *Proc. Natl Acad. Sci. USA* **98,** 2138–2141 (2001).
10. Gibb, E. L., Whittet, D. C. & Chiar, J. E. Searching for ammonia in grain mantles toward massive young stellar objects. *Astrophys. J.* **558,** 702–716 (2001).
11. Muñoz Caro, G. M., Ruiterkamp, R., Schutte, W. A., Greenberg, J. M. & Mennella, V. UV photodestruction of CH bonds and the evolution of the 3.4 μm feature carrier. I. The case of aliphatic and aromatic molecular species. *Astron. Astrophys.* **367,** 347–354 (2001).
12. Mennella, V. *et al.* UV photodestruction of CH bonds and the evolution of the 3.4 μm feature carrier. II. The case of hydrogenated carbon grains. *Astron. Astrophys.* **367,** 355–361 (2001).
13. Gerakines, P. A., Schutte, W. A., Greenberg, J. M. & van Dishoeck, E. F. The infrared band strengths of H_2O, CO and CO_2 in laboratory simulations of astrophysical ice mixtures. *Astron. Astrophys.* **296,** 810–818 (1995).
14. Gerakines, P. A. *et al.* Observations of solid carbon dioxide in molecular clouds with the infrared space observatory. *Astrophys. J.* **522,** 357–377 (1999).
15. Ehrenfreund, P. *et al.* Laboratory studies of thermally processed H_2O:CH_3OH:CO_2 ice mixtures and their astrophysical implications. *Astron. Astrophys.* **350,** 240–253 (1999).
16. Greenberg, J. M., Yencha, A. J., Corbell, J. W. & Frisch, H. L. in *Extrait de Mémoires de la Société Royale des Sciences de Liége* 425 (Société Royale des Sciences de Liége, Liége, 1972).
17. Briggs, R. *et al.* Comet Halley as an aggregate of interstellar dust and further evidence for the photochemical formation of organics in the interstellar medium. *Orig. Life Evol. Biosphere* **22,** 287–307 (1992).
18. Bernstein, M. P., Sandford, S. A., Allamandola, L. J., Chang, S. & Scharberg, M. A. Organic compounds produced by photolysis of realistic interstellar and cometary ice analogs containing methanol. *Astrophys. J.* **454,** 327–344 (1995).
19. Kobayashi, K. *et al.* Synthesis of amino acids in Earth orbit: Proposal. *Adv. Space Res.* **23,** 401–404 (1999).
20. Jenniskens, P. *et al.* Carbon dust formation on interstellar grains. *Astron. Astrophys.* **273,** 583–600 (1993).
21. Johns, R. B. & Seuret, M. G. Photochemistry of biological molecules. III. Mechanism of photodamage of alanine peptides in the solid state. *Photochem. Photobiol.* **12,** 405–417 (1970).
22. Huang, Z.-H., Wang, J., Gage, D. A., Watson, J. T. & Sweeley, C. C. Characterization of N-ethoxycarbonyl ethyl esters of amino acids by mass spectrometry. *J. Chromatogr.* **635,** 271–281 (1993).
23. Muñoz Caro, G. M., Meierhenrich, U. J., Schutte, W. A. & Greenberg, J. M. UV photoprocessing of interstellar ice analogs. Formation of HMT derivatives. *Astron. Astrophys.* (submitted).
24. Abe, I., Fujimoto, N., Nishiyama, T., Terada, K. & Nakahara, T. Rapid analysis of amino acid enantiomers by chiral-phase capillary gas chromatography. *J. Chromatogr. A* **722,** 221–227 (1996).
25. Kissel, J. & Krueger, F. R. The organic component in dust from comet Halley as measured by the PUMA mass spectrometer on board Vega 1. *Nature* **326,** 755–760 (1987).
26. Miller, S. L. A production of amino acids under possible primitive Earth conditions. *Science* **117,** 528–529 (1953).
27. Bernstein, M. P. *et al.* UV irradiation of polycyclic aromatic hydrocarbons in ices: production of alcohols, quinones, and ethers. *Science* **283,** 1135–1138 (1999).
28. Greenberg, J. M. in *Comets* (ed. Wilkening, L. L.) 131–163 (Univ. Arizona Press, Tucson, 1982).
29. Irvine, W. M., Schloerb, F. P., Crovisier, J., Fegley, B.Jr & Mumma, M. J. in *Protostars and Planets IV* (eds Mannings, V., Boss, A. P. & Russell, S. S.) 1159–1200 (Univ. Arizona Press, Tucson, 2000).
30. Chyba, C. & Sagan, C. Endogenous production, exogenous delivery and impact-shock synthesis of organic molecules: an inventory for the origins of life. *Nature* **355,** 125–131 (1992).
31. Weber, P. & Greenberg, J. M. Can spores survive in interstellar space?*Nature* **316,** 403–407 (1985).

Acknowledgements

We thank A. MacDermott, F. Goesmann and R. Roll for discussions and K. Getliffe for suggestions. Our collaboration was originally supported by the Max-Planck-Institut für Aeronomie at Katlenburg-Lindau with grants for G.M.M.C. and U.J.M., as preparatory work for the Rosetta mission. The work was performed at the Sackler Laboratory for Astrophysics at Leiden Observatory and the Centre Biophysique Moléculaire at Orléans, where it was funded by the European Union and by French sponsors: CNES, FNAD, Région Centre, and Département du Cher. In Orléans U.J.M. was supported by a Le Studium grant. U.J.M. is grateful for a habilitation grant by the Deutsche Forschungsgemeinschaft, and G.M.M.C. for an AIO allowance by Leiden University. This paper is dedicated to the memory of J.M.G., who died on 29 November 2001.

Competing interests statement

The authors declare that they have no competing financial interests.

Correspondence and requests for materials should be addressed to U.J.M. (e-mail: mhenrich@uni-bremen.de).

Exchange-biased quantum tunnelling in a supramolecular dimer of single-molecule magnets

Wolfgang Wernsdorfer*, Núria Aliaga-Alcalde†, David N. Hendrickson‡ & George Christou†

** Laboratoire Louis Néel-CNRS, BP166, 25 Avenue des Martyrs, 38042 Grenoble, Cedex 9, France*
† Department of Chemistry, University of Florida, Gainesville, Florida 32611-7200, USA
‡ Department of Chemistry, University of California at San Diego, La Jolla, California 92093-0358, USA

Various present and future specialized applications of magnets require monodisperse, small magnetic particles, and the discovery of molecules that can function as nanoscale magnets was an important development in this regard[1–3]. These molecules act as single-domain magnetic particles that, below their blocking temperature, exhibit magnetization hysteresis, a classical property of macroscopic magnets. Such 'single-molecule magnets' (SMMs)[4] straddle the interface between classical and quantum mechanical behaviour because they also display quantum tunnelling of magnetization[5,6] and quantum phase interference[7]. Quantum tunnelling of magnetization can be advantageous for some potential applications of SMMs, for example, in providing the quantum superposition of states required for quantum computing[8]. However, it is a disadvantage in other applications, such as information storage, where it would lead to information loss. Thus it is important to both understand and control the quantum properties of SMMs. Here we report a supramolecular SMM dimer in which antiferromagnetic coupling between the two components results in quantum behaviour different from that of the individual SMMs. Our experimental observations and theoretical analysis suggest a means of tuning the quantum tunnelling of magnetization in SMMs. This system may also prove useful for studying quantum tunnelling of relevance to mesoscopic antiferromagnets.

The compound $[Mn_4O_3Cl_4(O_2CEt)_3(py)_3]$ (hereafter Mn4) con-

tains three Mn^{3+} ions and one Mn^{4+} ion, and exchange coupling between them leads to Mn4 having a ground state spin of $S = 9/2$. Mn4 crystallizes in the hexagonal space group $R\bar{3}$ with pairs of Mn4 molecules lying 'head to head' on a crystallographic S_6 symmetry axis (Fig. 1)[9]. Thus, each Mn4 has C_3 symmetry and the $[Mn4]_2$ dimer has S_6 symmetry. This supramolecular arrangement is held together by six C–H···Cl hydrogen bonds (dashed lines in Fig. 1) between the pyridine rings on one [Mn4] and Cl ions on the other. C–H···X (where X is an electronegative atom) hydrogen bonds[10–12] are weaker than their O–H···X and N–H···X analogues but are nevertheless of fundamental importance in the packing of organic and inorganic molecules in the solid state, the folding of biomolecules, and a wide variety of molecular recognition events, crystal engineering, and similar types of interactions[13–15], particularly when X is O. The C–H···Cl hydrogen bonds in $[Mn4]_2$ have C···Cl distances and C–H···Cl angles of 3.71 Å and 161.57°, respectively, typical of this type of hydrogen bond[11,16,17]. The $[Mn4]_2$ dimer also brings the central bridging Cl ions of each [Mn4] close together (3.858 Å, dotted line in Fig. 1), almost at their van der Waals separation (~3.6 Å). Each $[Mn4]_2$ dimer is well separated from neighbouring dimers.

The supramolecular linkage within $[Mn4]_2$ introduces exchange interactions between the Mn4 molecules via both the six C–H···Cl pathways and the Cl···Cl approach. Most of the spin density at each Mn^{3+} ion is in d_π-orbitals, and some of this is known[9,18] to be delocalized into the pyridine π-system. Overlap with Cl π-orbitals of the neighbour provides an antiferromagnetic interaction. Similarly, the approach of the central Cl ions provides another pathway for antiferromagnetic exchange; propagation of the latter through metal-bound Cl ions is extremely well documented[19]. All seven interactions in $[Mn4]_2$ are expected to be weak, but combined they will lead to noticeable antiferromagnetic coupling between the Mn4 units.

The antiferromagnetic coupling between the Mn4 units in $[Mn4]_2$ makes this dimer an excellent candidate for studying quantum tunnelling in a system of truly identical, antiferromagnetically coupled particles with $S = 0$ ground states. Tunnelling studies were performed by magnetization measurements on single crystals using an array of micro-SQUIDs[20]. Figure 2 shows typical hysteresis loops in magnetization versus magnetic field scans with the field applied approximately along the easy axis of magnetization of $[Mn4]_2$, that is, approximately parallel to the S_6 axis. These loops display step-like features separated by plateaus. The step heights are temperature-dependent above 0.3 K; below this, the loops become temperature-independent. As discussed below, the steps are due to resonant quantum tunnelling of the magnetization (QTM) between the energy states of the $[Mn4]_2$ dimer. QTM has been previously observed for several SMMs[5–7,20–25], but what makes $[Mn4]_2$ unusual is that the QTM is now the collective behaviour of the complete $S = 0$ dimer of exchange-coupled $S = 9/2$ Mn4 quantum systems. This coupling is manifested as an exchange bias of all tunnelling transitions, and the hysteresis loops consequently display unique features, such as the absence for the first time in a SMM of a QTM step at zero field.

Before interpreting the hysteresis loops further, we present a

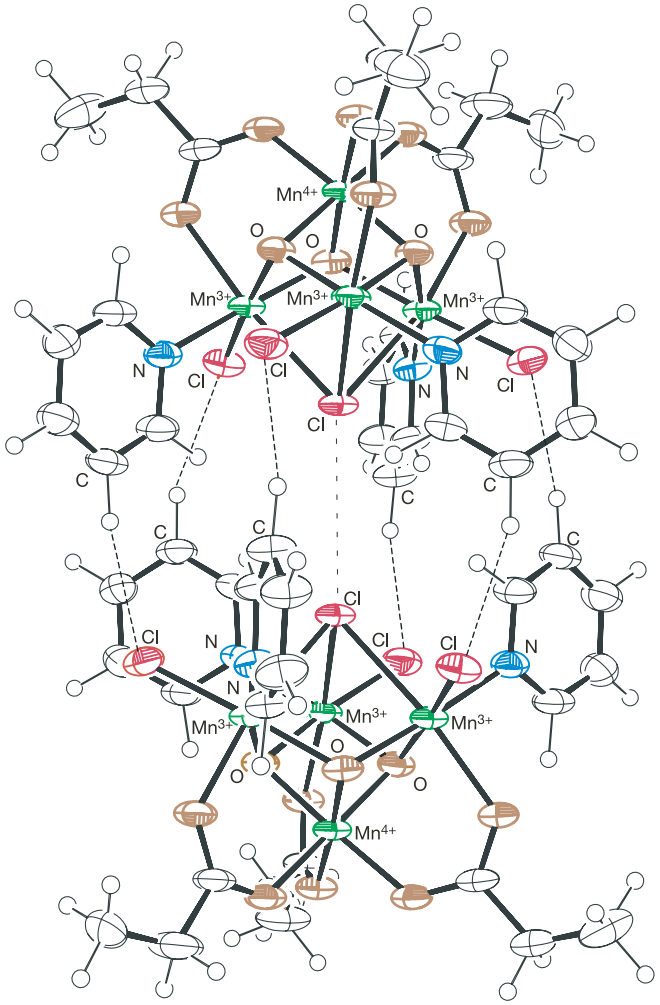

Figure 1 The structure of the $[Mn_4O_3Cl_4(O_2CEt)_3(py)_3]_2$ dimer, denoted $[Mn4]_2$. The small circles are hydrogen atoms. The dashed lines are C–H···Cl hydrogen bonds and the dotted line is the close Cl···Cl approach. Brown, oxygen; green, manganese; red, chlorine; blue, nitrogen; py, pyridine.

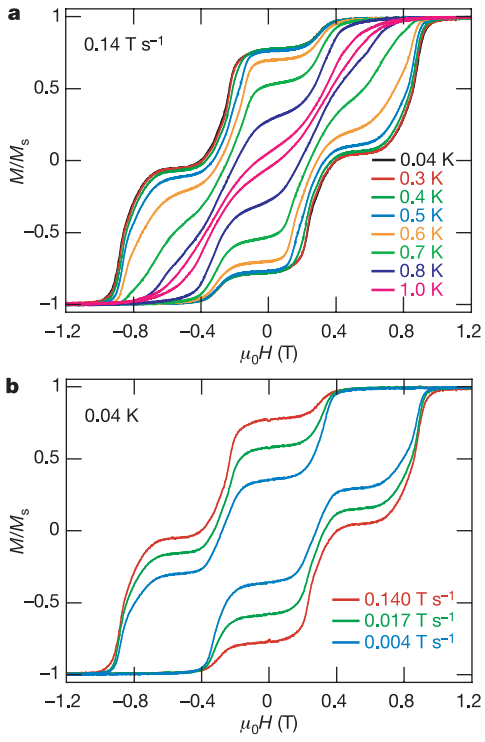

Figure 2 Magnetization (M) of $[Mn4]_2$ (plotted as fraction of maximum value M_s) versus applied magnetic field ($\mu_0 H$). **a**, **b**, The resulting hysteresis loops are shown at different temperatures (**a**) and different field sweep rates (**b**). We note that the loops become temperature-independent below about 0.3 K but are still sweep-rate-dependent owing to resonant quantum tunnelling between discrete energy states of the $[Mn4]_2$ dimer.

simplified spin hamiltonian describing the $[Mn4]_2$ dimer. Each Mn4 can be modelled as a 'giant spin' of $S = 9/2$ with Ising-like anisotropy. The corresponding hamiltonian (H_i) is given by equation (1)

$$H_i = D\hat{S}_{zi}^2 + H_i^{trans} + g\mu_B\mu_0\hat{S}_{zi}H_z \quad (1)$$

where $i = 1$ or 2 (referring to the two Mn4 SMMs of the dimer), D is the axial anisotropy constant, μ_B is the Bohr magneton, $\hat{S}_z$ is the easy-axis spin operator, g is the electronic g-factor, μ_0 is the vacuum permeability, and H_z is the applied longitudinal field. The exact form of the transverse anisotropy H_i^{trans} is not important in this discussion. The last term in equation (1) is the Zeeman energy associated with an applied field. The Mn4 units within $[Mn4]_2$ are coupled by a weak superexchange, J, via both the six C–H···Cl pathways and the Cl···Cl approach. Thus, the hamiltonian (H) for $[Mn4]_2$ is

$$H = H_1 + H_2 + J\hat{S}_1\hat{S}_2 \quad (2)$$

where $S_1 = S_2 = 9/2$. Tunnelling among the $(2S_1 + 1)(2S_2 + 1) = 100$ energy states is allowed by the small transverse anisotropy H_i^{trans} and the transverse coupling terms containing $\hat{S}_{xi}$ and $\hat{S}_{yi}$ operators. The energy states of $[Mn4]_2$ can easily be calculated by exact diagonalization; however, for simplicity, all transverse anisotropy terms were neglected. Each state of $[Mn4]_2$ can then be labelled by two quantum numbers (M_1, M_2) for the two Mn4 SMMs, with $M_1 = 9/2, 7/2, \ldots, -9/2$ and $M_2 = 9/2, 7/2, \ldots, -9/2$. The energy states are plotted in Fig. 3a as a function of applied field.

At very low temperature, most of the excited spin states are not populated and can be neglected. Thus, Fig. 3b shows only the low-lying states involved in the magnetization reversal at very low temperature when sweeping the field from a high negative field to a positive one. At high negative field, the initial state is $(M_1, M_2) = (-9/2, -9/2)$, that is, both molecules are in the negative ground state. As the magnetic field is swept, the first (avoided) level crossing is at −0.33 T. There is a non-zero probability, which depends upon the sweep rate, for the magnetization to tunnel from $(-9/2, -9/2)$ to $(-9/2, 9/2)$. (For convenience, we do not list here both degenerate (M, M') and (M', M) states.) The smaller the sweep rate the larger is the tunnelling probability, that is, the larger is the resulting step in Fig. 2b. At field values away from the avoided level crossing, the dimer states are frozen by the significant magnetic anisotropy barrier.

At the next level crossing at 0 T, there is the possibility of tunnelling from $(-9/2, -9/2)$ to $(9/2, 9/2)$, but this requires both Mn4 molecules of the dimer to tunnel simultaneously. The corresponding tunnelling probability is very small and can be neglected. Between 0.15 and 0.75 T, there are several level crossings from $(-9/2, -9/2)$ to excited states (shown only in Fig. 3a) that require simultaneous tunnelling in both Mn4 units and will not be discussed further. At the next level crossing at 0.2 T, $[Mn4]_2$ can undergo tunnelling from $(-9/2, -9/2)$ to $(-9/2, 7/2)$, corresponding to one of the Mn4 molecules tunnelling from the ground state to an excited state, followed by rapid relaxation from $(-9/2, 7/2)$ to $(-9/2, 9/2)$ (curly arrow in Fig. 3b). At the next level crossing at 0.33 T, the situation is analogous to that at −0.33 T, and the dimer can undergo tunnelling from $(-9/2, 9/2)$ to $(9/2, 9/2)$. The level crossing at 0.75 T allows tunneling from $(-9/2, -9/2)$ to $(-9/2, 5/2)$, followed by relaxation from $(-9/2, 5/2)$ to $(-9/2, 7/2)$ and $(-9/2, 9/2)$. Finally, at 0.87 T tunnelling can occur from $(-9/2, 9/2)$ to $(7/2, 9/2)$, followed by relaxation from $(7/2, 9/2)$ to $(9/2, 9/2)$.

The values of D and J used in Fig. 3 were calculated from the field positions of the steps in the hysteresis loops, ignoring transverse (and fourth order) terms; the positions were determined from the first derivative (Fig. 4). We note that closely spaced peaks are not well resolved, owing to broadening by dipolar and transverse fields, and possibly other effects; this and the variation in broadnesses are under further study. The calculated values are $D = -0.72$ K and $J = +0.1$ K. The former is very close to those determined experimentally for several (isolated) Mn4 SMMs[23,26], and the latter is

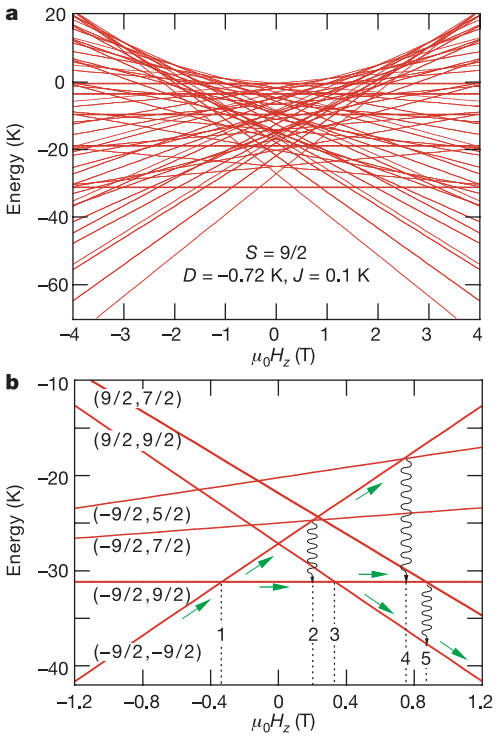

Figure 3 The spin state energies of $[Mn4]_2$ as a function of applied magnetic field. **a**, Energy versus magnetic field plot for the 100 states of the exchange-coupled dimer of two spin $S = 9/2$ Mn4 units. Transverse terms in equations (1) and (2) are neglected for the sake of simplicity. **b**, Enlargement of **a**, showing only levels populated at very low temperature when the field is swept from −1.2 T to +1.2 T, as indicated by green arrows. Dotted lines, labelled 1 to 5, indicate the strongest tunnel resonances: 1, $(-9/2, -9/2)$ to $(-9/2, 9/2)$; 2, $(-9/2, -9/2)$ to $(-9/2, 7/2)$, followed by relaxation to $(-9/2, 9/2)$; 3, $(-9/2, 9/2)$ to $(9/2, 9/2)$; 4, $(-9/2, -9/2)$ to $(-9/2, 5/2)$, followed by relaxation to $(-9/2, 9/2)$; 5, $(-9/2, 9/2)$ to $(7/2, 9/2)$, followed by relaxation to $(9/2, 9/2)$. For clarity, degenerate states such as (M,M') and (M',M) are not listed. S, spin value; D, axial anisotropy constant; J, superexchange parameter.

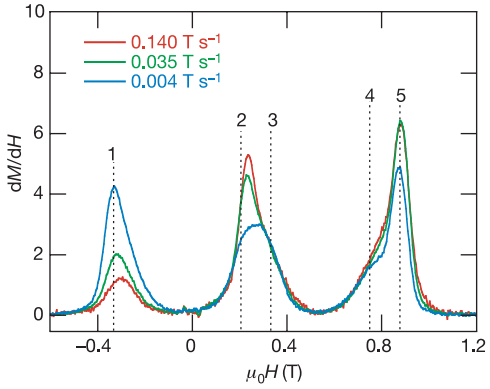

Figure 4 Derivative of the hysteresis loop at 0.04 K (Fig. 2b) and at different field sweep rates. The dominating tunnel transitions are indicated by dashed lines and numbers 1 to 5, which are indicated in Fig. 3b and explained in the text. The dashed lines are at positions calculated from Fig. 3b (which ignores transverse terms in equations (1) and (2), as well as fourth-order terms). M, magnetization; H, field.

antiferromagnetic (positive value) and very weak, as expected for an exchange interaction via the six C–H···Cl and the Cl···Cl pathways. A value of $J \approx 0.1$ K was also obtained from d.c. susceptibility measurements in the 1 to 8 K range.

The above results demonstrate that even weak exchange interactions can have a large influence of the quantum properties of SMMs. From one viewpoint, each half of the $[Mn4]_2$ dimer acts as a field bias on its neighbour, shifting the tunnel resonances to new positions relative to isolated Mn4 molecules. In particular, these single Mn4 molecules show a strong QTM step at zero field in the hysteresis loop[23], a feature absent for $[Mn4]_2$ (Fig. 2) because this would be a double quantum transition with a very low probability of occurrence. The absence of tunnelling at zero field is important if SMMs are to be used for information storage, and the option is still retained to switch on tunnelling, if and when required, by application of a field. Thus, future studies will investigate this double transition at zero field in $[Mn4]_2$, and the corresponding multiple quantum transition in higher supramolecular aggregates of SMMs, and determine their exact probability of occurrence and to what extent this can be controlled by the degree of aggregation, variation of exchange coupling strength and similar modifications. From another viewpoint, $[Mn4]_2$ represents an example of quantum tunnelling within a monodisperse antiferromagnetically coupled particle with no uncompensated spin (that is, $S = 0$) in the ground state. It may also prove possible to study its $(9/2, -9/2)$ to $(-9/2, 9/2)$ tunnelling transition. This would be analogous to the transition in antiferromagnets, in which tunnelling is predicted[27] to be more pronounced than in ferromagnets. Such a study for ferritin suffered from the practical impossibility of having all molecules in the sample be the same size, and possess completely compensated spins[28–30]. Finally, the absence of a level crossing at zero field also makes $[Mn4]_2$ a very interesting candidate as a qubit for quantum computing[8], because its ground state is the entangled combination of the $(9/2, -9/2)$ and $(-9/2, 9/2)$ states; the coupling of this $S = 0$ system to environmental degrees of freedom should be small, which means decoherence effects should also be small.

In future work, we shall use the Landau–Zener method[20] to determine the tunnel splitting in $[Mn4]_2$, and apply a transverse field to probe its exact influence on QTM rates (we have already confirmed that a transverse field increases the tunnelling rate, as expected for QTM). The identification of both an antiferromagnetic coupling and an exchange-bias effect in $[Mn4]_2$ demonstrates the feasibility of employing supramolecular chemistry to modulate the quantum physics of SMMs, providing a realistic method for fine-tuning the properties of these molecular nanoscale materials. This brings closer their use in devices.

Received 29 October 2001; accepted 13 February 2002.

1. Sessoli, R. *et al.* High-spin molecules: $[Mn_{12}O_{12}(O_2CR)_{16}(H_2O)_4]$. *J. Am. Chem. Soc.* **115,** 1804–1816 (1993).
2. Sessoli, R., Gatteschi, D., Caneschi, A. & Novak, M. A. Magnetic bistability in a metal-ion cluster. *Nature* **365,** 141–143 (1993).
3. Christou, G., Gatteschi, D., Hendrickson, D. N. & Sessoli, R. Single-molecule magnets. *MRS Bull.* **25,** 66–71 (2000).
4. Aubin, S. M. J. *et al.* Distorted $Mn^{IV}Mn^{III}_3$ cubane complexes as single-molecule magnets. *J. Am. Chem. Soc.* **118,** 7746–7754 (1996).
5. Friedman, J. R., Sarachik, M. P., Tejada, J. & Ziolo, R. Macroscopic measurement of resonant magnetization tunnelling in high-spin molecules. *Phys. Rev. Lett.* **76,** 3830–3833 (1996).
6. Thomas, L. *et al.* Macroscopic quantum tunneling of magnetization in a single crystal of nanomagnets. *Nature* **383,** 145–147 (1996).
7. Wernsdorfer, W. & Sessoli, R. Quantum phase interference and parity effects in magnetic molecular clusters. *Science* **284,** 133–135 (1999).
8. Leuenberger, M. N. & Loss, D. Quantum computing in molecular magnets. *Nature* **410,** 789–793 (2001).
9. Hendrickson, D. N. *et al.* Photosynthetic water oxidation center: spin frustration in distorted cubane $Mn^{IV}Mn^{III}_3$ model complexes. *J. Am. Chem. Soc.* **114,** 2455–2471 (1992).
10. Desiraju, G. R. The C–H···O hydrogen bond: structural implications and supramolecular design. *Acc. Chem. Res.* **29,** 441–449 (1996).
11. Freytag, M. & Jones, P. G. Hydrogen bonds C–H···Cl as a structure-determining factor in the gold(I) complex bis(3-bromopyridine)gold(I) dichloroaurate(I). *Chem. Commun.* 277–278 (2000).
12. Aullón, G., Bellamy, D., Brammer, L., Bruton, E. A. & Orpen, A. G. Metal-bound chlorine often accepts hydrogen bonds. *Chem. Commun.* 653–654 (1998).
13. Raymo, F. M., Bartberger, M. D., Houk, K. N. & Stoddart, J. F. The magnitude of [C–H···O] hydrogen bonding in molecular and supramolecular assemblies. *J. Am. Chem. Soc.* **123,** 9264–9267 (2001).
14. Jeffrey, G. A. & Saenger, W. *Hydrogen Bonding in Biological Structures* (Springer, Berlin, 1991).
15. Desiraju, G. R. *Crystal Engineering: the Design of Organic Solids* (Elsevier, Amsterdam, 1989).
16. Jones, P. G. & Ahrens, B. Bis(diphenylphosphino)methane and related ligands as hydrogen bond donors. *Chem. Commun.* 2307–2308 (1998).
17. Xu, C. *et al.* Synthesis, molecular structures and fluxional behavior of dppm-bridged complexes of platinum(II) with linear gold(I), trigonal silver(I), or tetrahedral mercury(II) centers. *Organometallics* **15,** 3972–3979 (1996).
18. Wemple, M. W., Tsai, H.-L., Folting, K., Hendrickson, D. N. & Christou, G. Distorted cubane $[Mn_4O_3Cl]^{6+}$ complexes with arenecarboxylate ligation: crystallographic, magnetochemical and spectroscopic characterization. *Inorg. Chem.* **32,** 2025–2031 (1993).
19. Carlin, R. L. *Magnetochemistry* (Springer, Berlin, 1986).
20. Wernsdorfer, W. Classical and quantum magnetization reversal studies in nanometer-sized particles and clusters. *Adv. Chem. Phys.* **118,** 99–190 (2001).
21. Sangregorio, C. *et al.* Quantum tunnelling of the magnetization in an iron cluster nanomagnet. *Phys. Rev. Lett.* **78,** 4645–4648 (1997).
22. Aubin, S. M. J. *et al.* Half-integer-spin, single-molecule magnet exhibiting resonant magnetization tunnelling. *J. Am. Chem. Soc.* **120,** 839–840 (1998).
23. Aubin, S. M. J. *et al.* Resonant magnetization tunnelling in the trigonal pyramidal $Mn^{IV}Mn^{III}_3$ complex $[Mn_4O_3Cl(O_2CMe)_3(dbm)_3]$. *J. Am. Chem. Soc.* **120,** 4991–5004 (1998).
24. Aubin, S. M. J. *et al.* Resonant magnetization tunnelling in the half-integer-spin single-molecular magnet $[PPh_4][Mn_{12}O_{12}(O_2CEt)_{16}(H_2O)_4]$. *Chem. Commun.* 803–804 (1998).
25. Boskovic, C., Pink, M., Huffman, J. C., Hendrickson, D. N. & Christou, G. Single-molecule magnets: ligand-induced core distortion and multiple Jahn–Teller isomerism in $[Mn_{12}O_{12}(OAc)_8(O_2PPh_2)_8(H_2O)_4]$. *J. Am. Chem. Soc.* **123,** 9914–9915 (2001).
26. Andres, H. *et al.* Inelastic neutron scattering and magnetic susceptibilities of the single-molecule magnets $[Mn_4O_3X(OAc)_3(dbm)_3$ (X = Br, Cl, OAc, and F): variation of the anisotropy along the series. *J. Am. Chem. Soc.* **122,** 12469–12477 (2000).
27. Barbara, B. & Chudnovsky, E. M. Macroscopic quantum tunneling in antiferromagnets. *Phys. Lett. A* **145,** 205–208 (1990).
28. Awschalom, D. D., Smyth, J. F., Grinstein, G., DiVincenzo, D. P. & Loss, D. Macroscopic quantum tunneling in magnetic proteins. *Phys. Rev. Lett.* **68,** 3092–3095 (1992).
29. Gider, S., Awschalom, D. D., Douglas, T., Mann, S. & Chaparala, M. Classical and quantum magnetic phenomena in natural and artificial ferritin proteins. *Science* **268,** 77–80 (1995).
30. Tejada, J. *et al.* Does macroscopic quantum coherence occur in ferritin?*Science* **272,** 424–426 (1996).

Acknowledgements

We thank the US National Science Foundation for support. We also thank A. Benoit, D. Mailly and C. Thirion for help in the development of the micro-SQUID technique, and B. Barbara for his support.

Competing interests statement

The authors declare that they have no competing financial interests.

Correspondence and requests for materials should be addressed to G.C. (e-mail: christou@chem.ufl.edu).

Molecular dynamics simulation of the ice nucleation and growth process leading to water freezing

Masakazu Matsumoto, Shinji Saito & Iwao Ohmine

Chemistry Department, Nagoya University, Chikusa-ku, Nagoya, Japan 464-8602

Upon cooling, water freezes to ice. This familiar phase transition occurs widely in nature, yet unlike the freezing of simple liquids[1–3], it has never been successfully simulated on a computer. The difficulty lies with the fact that hydrogen bonding between individual water molecules yields a disordered three-dimensional hydrogen-bond network whose rugged and complex global potential energy surface[4–6] permits a large number of possible network configurations. As a result, it is very challenging to reproduce the freezing of 'real' water into a solid with a unique crystalline structure. For systems with a limited number of possible disordered hydrogen-bond network structures, such as